BIOCHEMISTRY

Single-molecule observation of nucleotide induced conformational changes in basal SecA-ATP hydrolysis

Nagaraju Chada[1]*, Kanokporn Chattrakun[1], Brendan P. Marsh[1†], Chunfeng Mao[2], Priya Bariya[2], Gavin M. King[1,2‡]

SecA is the critical adenosine triphosphatase that drives preprotein transport through the translocon, SecYEG, in *Escherichia coli*. This process is thought to be regulated by conformational changes of specific domains of SecA, but real-time, real-space measurement of these changes is lacking. We use single-molecule atomic force microscopy (AFM) to visualize nucleotide-dependent conformations and conformational dynamics of SecA. Distinct topographical populations were observed in the presence of specific nucleotides. AFM investigations during basal adenosine triphosphate (ATP) hydrolysis revealed rapid, reversible transitions between a compact and an extended state at the ~100-ms time scale. A SecA mutant lacking the precursor-binding domain (PBD) aided interpretation. Further, the biochemical activity of SecA prepared for AFM was confirmed by tracking inorganic phosphate release. We conclude that ATP-driven dynamics are largely due to PBD motion but that other segments of SecA contribute to this motion during the transition state of the ATP hydrolysis cycle.

INTRODUCTION

More than 30% of newly synthesized proteins in *Escherichia coli* are exported across the cytoplasmic membrane to their final destinations, where they acquire their natively folded and functional state (*1*, *2*). Several distinct export mechanisms have evolved to accomplish this protein maneuvering, but only the general secretory (Sec) system is found in all domains of life. Proteins to be exported are synthesized as precursors with an N-terminal leader sequence and are translocated through the Sec pathway in *E. coli*. SecA, the adenosine triphosphatase (ATPase) of the Sec system, binds to the translocon SecYEG to form a translocase. In a process that is currently not well understood, this complex mediates chemomechanical conversion that results in translocation of precursor proteins across the cytoplasmic membrane (*3*, *4*).

Peripheral membrane protein SecA is a large multidomain protein (901 aminoacyl residues; Fig. 1A) with numerous binding partners including the translocon SecYEG, chaperone SecB, precursor proteins, and lipids (*5*–*8*). The multiple and complex functions that this macromolecule performs in a cell have likely led to the remarkable dynamics and flexibility that the domains of SecA exhibit (*1*, *9*). For example, the precursor-binding domain (PBD) is thought to move approximately 80° relative to other domains (Fig. 1B). Several models have been proposed to explain protein translocation with different roles for SecA, and interdomain allosteric regulation of ATPase activity is a common theme among them (*1*). SecA acts as a processive motor in a "piston" model where extended precursor protein segments move along its clamp (*10*, *11*). The tip of the two-helix finger [alternatively referred to as intramolecular regulator of ATPase (IRA1); Fig. 1, A and C, orange] has been proposed to latch onto the preprotein chain and push it through the SecYEG pore. The precursor is then translocated through the channel via adenosine triphosphate (ATP) hydrolysis–driven power strokes in a stepwise fashion (*4*, *12*). In another model, SecA controls SecYEG pore opening and closing through ATP hydrolysis, hence acting as an allosteric channel regulator. This facilitates a Brownian ratchet mechanism where the precursor protein undergoes proton motive force driven diffusion through the SecYEG channel, and SecA acts as a "brake" to prevent backsliding (*3*, *13*).

How SecA harnesses the energy released during ATP hydrolysis and translates it into functional conformational transitions to drive precursor protein chains through the translocon remains unclear. Major insight has come from x-ray crystallographic studies (*14*, *15*). The N-terminal portion of SecA consists of three large domains, namely two nucleotide-binding folds [Fig. 1, A (red, NBD1; blue, NBD2) and B (gray)] and the PBD (Fig. 1, A to C, pink). ATP binds at the interface of NBD1 and NBD2, forming a superfamily 2 helicase motor (*1*). The energy released during hydrolysis has been proposed to allosterically mobilize the PBD and the C-terminal segment [which includes most of the helical scaffold domain (HSD) and all of the helical wing domain to the C terminus; Fig. 1, B and C (crimson) (residues 620 to 901)] (*2*, *9*). SecA has been crystallized in the presence of different nucleotides and has exhibited three major conformational states: wide-open, open, and closed (Fig. 1B). It has thus been hypothesized that the PBD of SecA can swivel from wide-open to a closed state in a ligand-dependent manner (*1*, *10*, *14*, *16*, *17*).

A complementary line of inquiry to the static crystal structures would be to observe the conformational motions of SecA molecules during ATP hydrolysis in real time and in near-native conditions. Because these motions are triggered by stochastic events, they are asynchronous and challenging to resolve. Atomic force microscopy (AFM) is a single-molecule imaging technique that is well suited to these measurements. AFM uses an extremely sharp tip to probe protein topography and has proven useful in a number of biological contexts, primarily because it achieves molecular resolution imaging in solution in real time without the need for freezing or crystallization and with minimal molecular weight constraints (*18*, *19*). Despite its strengths, AFM generally requires proteins to be adsorbed to a supporting surface; this specimen preparation step can

[1]Department of Physics and Astronomy, University of Missouri–Columbia, Columbia, MO 65211, USA. [2]Department of Biochemistry, University of Missouri–Columbia, Columbia, MO 65211, USA.
*Present address: Department of Biology, Johns Hopkins University, 3400 North Charles Street, Baltimore, MD 21218, USA.
†Present address: Department of Applied Physics, Stanford University, Stanford, CA 94305 USA.
‡Corresponding author. Email: kinggm@missouri.edu

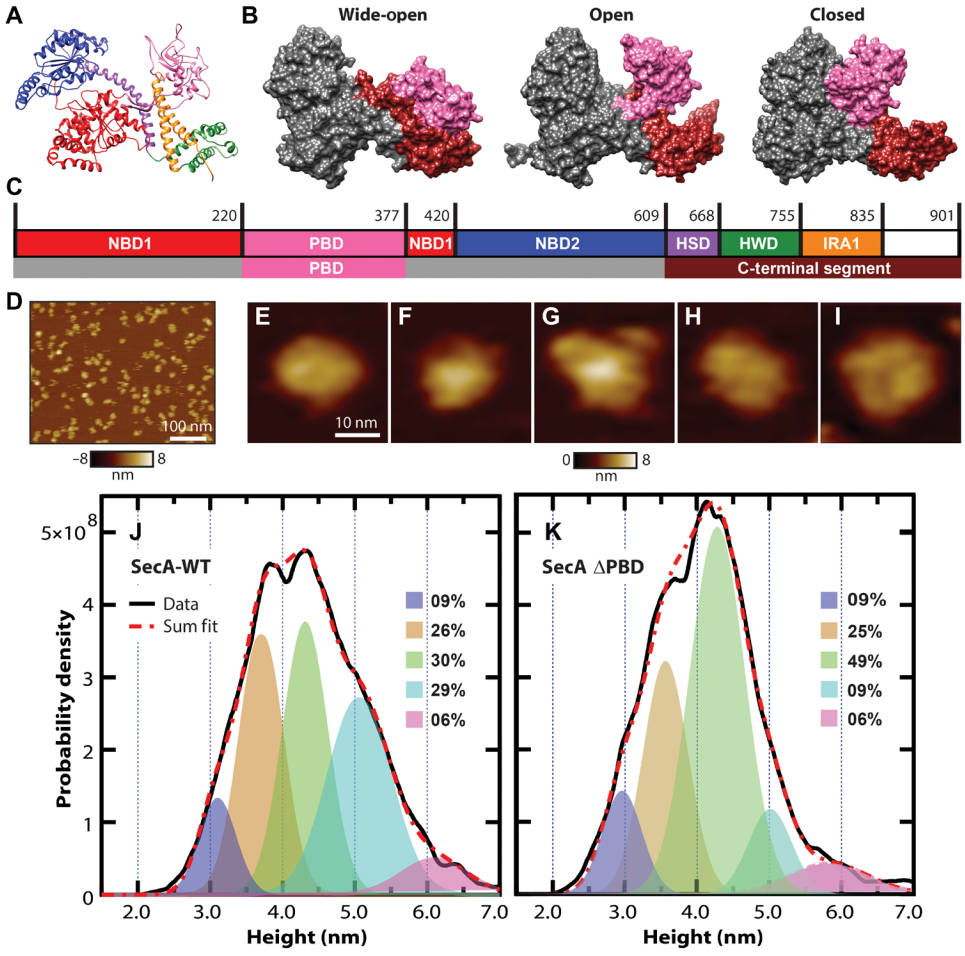

Fig. 1. Overview of SecA conformations and AFM data. (**A**) Structure of SecA [Protein Data Bank (PDB) code: 2FSF] in ribbon representation with the PBD modeled in from *Bacillus subtilis* (1TF5). (**B**) Different conformational states (*1,10,14,16*). The wide-open state obtained from *B. subtilis* (1M6N; left), open state from *B. subtilis* (1TF5; middle), and closed state from *Thermotoga maritima* (3DIN; right) are shown. The PBD and C domain are pink and crimson, respectively; all other domains are gray. (**C**) Color-coded domains in top band correspond to (A) and bottom band to (B). (**D**) AFM image of SecA-WT and (**E** to **I**) a series of detailed views exhibiting conformational differences. (**J**) Height distribution of SecA-WT (black solid line; number of different complexes that were measured $n = 3726$) showing multiple subpopulations. Five Gaussian fits with relative weights and the sum thereof (red dashed) are also shown. (**K**) Analogous data and fitting for the mutant SecAΔPBD (experiment: black, $n = 4009$; sum fit: red dashed). Note the reduction of the population at 5.1 nm in the case of the mutant. We chose to fit to five Gaussians because this number coincides with the number of prominent convex regions (populations) within the WT distribution; this number led to coefficient of determination (R^2) values of >0.997 for both SecA-WT and SecAΔPBD.

raise questions about activity. In principle, the product of surface-adsorbed enzymes can be measured to provide biochemical verification of activity.

Previously, our group applied AFM to study the translocon and translocase complexes in supported lipid bilayers. We measured the dynamics of the membrane external cytoplasmic loops of SecYEG and observed the association and dissociation of SecA with the translocon (*7*, *20*, *21*). Here, we apply single-molecule AFM imaging to study the conformational dynamics associated with basal SecA ATP hydrolysis and elucidate nucleotide-coupled conformational states. To focus on basal activity, SecA was passively adsorbed onto mica surfaces in the absence of binding partners. This also improves precision, as lipid bilayers can add noise to the measurement, for example, through vertical conformational fluctuations (*21*). We demonstrate angstrom-scale changes in protein conformations that correlate with particular domains and particular nucleotide species. Conformational changes were captured in real time at the single-molecule level with up to ~100-ms temporal resolution in physiological solution. Biochemical measurements tracking the release of radiolabeled γ-phosphate confirmed that the surface-adsorbed SecA prepared for AFM measurements still hydrolyzed ATP. Together, our work demonstrates through single-molecule observation that ATP hydrolysis drives large-scale conformational changes of specific domains of SecA.

RESULTS

We shed light on the conformational dynamics of SecA during ATP hydrolysis by imaging single molecules in near-native conditions. Following previous work (*7*, *20*, *21*), proteins were adsorbed to freshly cleaved mica and imaged via tapping mode AFM in aqueous solution. Salient topographic information, including the height and area of individual macromolecules, was extracted algorithmically and collected for statistical analyses (*22*).

We studied first wild-type SecA (SecA-WT). SecA-WT exists in equilibrium between monomer and dimer in *E. coli*. We focused on conformational dynamics of SecA monomer by choosing solution conditions that bias the system away from dimer (*23*). Figure 1D shows an AFM image of about 100 SecA-WT molecules. Detailed topographic images of individual proteins are also shown [Fig. 1, E to I; fig. S1 shows phase images (*24*)]. Simulated AFM images were constructed using x-ray crystal coordinates in conjunction with an assumed tip geometry (see Materials and Methods for details). Simulated images showed good overall agreement with the experimental data, and analysis implied that the orientation of the SecA on the mica was not random but had two preferred orientations (figs. S2 and S3).

We determined the relationship between specific topographical populations and the functionally important PBD of SecA. The distribution of feature height for individual SecA-WT molecules in the apo state (i.e., not exposed to any nucleotide after purification) is presented (Fig. 1J, black). These data show that most of the conformations exhibit a maximum height of around 4 nm. A closer inspection reveals a minimum separating two subpopulations that are spaced ~0.5 nm apart. Although small, this separation is above the ~0.1-nm vertical resolution of the technique (*25*). Figure S4 demonstrates that the separation between the two peaks is robust. We observed an additional subpopulation in the height distribution as a distinct shoulder at about 5.1 nm (Fig. 1J, light blue shade). This shoulder population was substantial, comprising 29% of the total. When a variant of SecA with the PBD deleted (SecAΔPBD) was analyzed, the population at 5.1 nm was diminished significantly (Fig. 1K, light blue shade). At the same time, the population at 4.3 nm was enhanced by roughly the same amount (compare Fig. 1, J and K, green shades), and the other three populations were essentially unchanged compared to the WT enzyme (Fig. 1, J and K; dark blue, orange, and pink shades). We emphasize that the peak positions of the two major populations match exactly; hence, SecA-WT and the mutant lacking the PBD are likely to be in the same overall orientation on the mica. This notion is buttressed by similarities in equipotential surface maps between the two SecA species (fig. S5). Hence, the conformational state at 5.1 nm appears to be directly related to the PBD. We note that cells require the PBD of SecA; SecAΔPBD was overproduced, and the purified sample contained <10% residual SecA-WT.

Before characterizing enzyme topography during ATP hydrolysis, we sought to verify the ATPase activity of SecA samples as prepared for AFM study. To this end, we performed thin-layer chromatography to track the dephosphorylation of [γ-^{32}P]-labeled ATP. The approach was based on prior work (*26*) modified to probe surface-adsorbed enzymes. We prepared SecA-WT samples on mica in a manner identical to that used for AFM imaging, but at a higher concentration (2.4 μM) to increase the signal. At this concentration, most of the SecA will be dimer [K_d (dissociation constant) ≤ 1 μM] (*2*); however, basal ATPase activity of SecA is weakly coupled to oligomeric state (*27*). The generation of inorganic phosphate (Pi) from mica-adsorbed SecA-WT over time is shown (Fig. 2). We carried out control experiments on mica in the absence of SecA. The results show that SecA actively hydrolyzes ATP when adsorbed to mica, even over extended time periods (>2 hours) that are frequently used for AFM study.

What fraction of the SecA molecules retained ATPase activity when bound to the mica surface? To estimate this, we used AFM data and molecular dimensions to determine that approximately 3×10^{-12} mol of SecA was available on the mica disk during the surface-adsorbed ATPase assay (fig. S6). Figure 2C shows a time course of mol ATP hydrolyzed divided by mol SecA available. The slope represents the normalized ATP turnover rate. For comparison, we carried out a traditional solution-based assay with SecA at a monomer concentration of 2.4 μM (Fig. 2D). The results indicate that there is only a modest decrease of 6% in activity when the molecules are adsorbed onto mica. This unexpected result suggests that approximately 9 of 10 SecA molecules remain active for ATP turnover when adsorbed on mica. We note that, in addition to the aforementioned estimate of SecA copy number, there are other uncertainties in this result. For example, it is possible that the surface itself can act as a mild destabilization agent; it has been shown that low levels of the denaturant urea stimulate the ATPase activity of SecA (*28*). In the face of caveats, our results suggest that a significant fraction of SecA molecules remain competent for ATP hydrolysis when adsorbed onto mica for AFM analysis.

After confirming that ATPase activity was maintained, we studied the dynamic topography of SecA during ATP hydrolysis. The SecA-WT and the SecAΔPBD mutant were subjected to four different ATP assays: (i) apo (Fig. 3, black); (ii) preincubated with 100 μM ATP for 15 min before deposition on mica and then imaged in the absence of ATP (Fig. 3, red); (iii) preincubated with 100 μM ATP in solution for 15 min and then imaged with 100 μM ATP in the imaging buffer (Fig. 3, green); and last, to monitor the long time-scale recovery of the enzyme after ATP exposure; (iv) preincubated with 100 μM ATP in solution for 4 hours and then imaged in the absence of ATP in the imaging buffer (Fig. 3, blue). The concentration of ATP chosen for this study was significantly higher than the reported affinity for ATP (K_d ~ 300 nM) (*29*). Representative images of SecA-WT and SecAΔPBD from the four assays are shown (fig. S7).

We determined the footprint area of each protein (i.e., the area the macromolecules projected onto the local background). These footprint area distributions are presented as smoothed histograms in Fig. 3 [A (SecA-WT) and C (SecAΔPBD)]. When exposed to ATP, the areal footprint of SecA-WT increased in all conditions studied [compare primary peak position for the apo state of 200 nm^2 (black) to 270 nm^2 (red), 300 nm^2 (green), and 280 nm^2 (blue); Fig. 3A]. The observation of increased area suggests that SecA-WT explores a wider conformational space upon ATP exposure. Furthermore, the area increases remained 4 hours after ATP exposure; hence, the ATP-induced changes were persistent.

In contrast to SecA-WT, three of the four principal populations of the SecAΔPBD footprint area remained essentially unchanged after ATP exposure [compare the primary peak position of 230 nm^2 (black) to 230 nm^2 (red) and 235 nm^2 (blue); Fig. 3C]. This implies that the aforementioned increases in the area observed for SecA-WT are due to PBD motion. We note that SecA lacking the PBD still hydrolyzes ATP (*30*). Hence, an overall destabilization of the macromolecule due to the energy released upon ATP hydrolysis can be ruled out. The primary peak observed at 300 nm^2 in the case of the SecAΔPBD mutant when imaged in the presence of ATP (Fig. 3C, green) could be attributable to motion of the NBD1 and NBD2 domains, but we think that it is more likely to be the C-terminal segment that moves. The C-terminal segment of SecA has been shown to be highly mobile and is thought to be an additional regulator of ATP hydrolysis that inserts into membrane during translocation (*9*, *17*). Statistics of the area footprint distributions and heights for SecA-WT and SecAΔPBD in different conditions are presented (see tables S1 to S4).

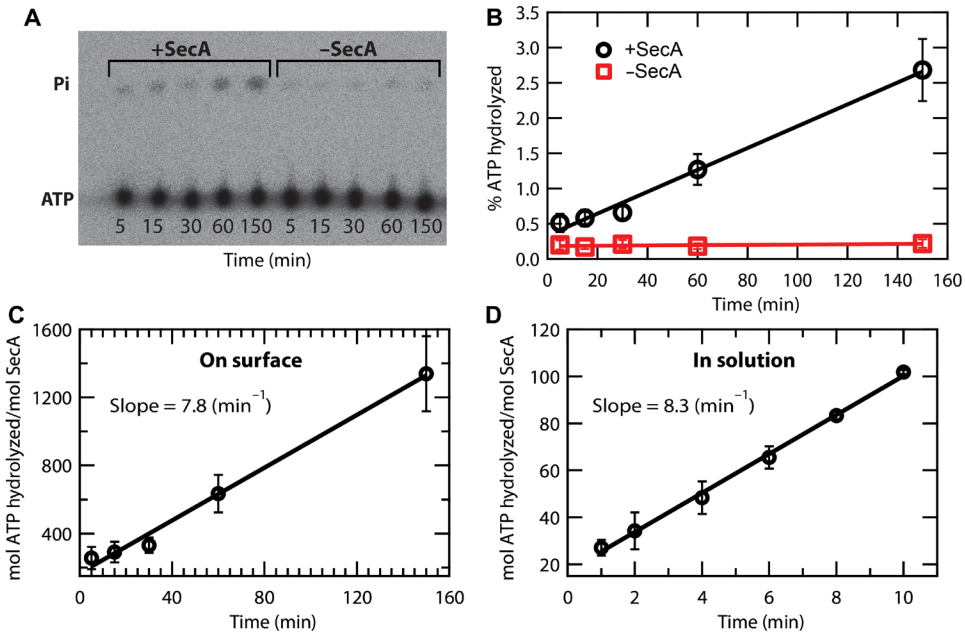

Fig. 2. ATPase activity of surface-adsorbed SecA and comparison with traditional solution assay. (**A**) Image of radioactivity showing the generation of ^{32}Pi from ATP. (**B**) Quantification of percent ATP hydrolysis over time in the presence (circles) and absence (squares) of SecA. (**C**) Amount of ATP hydrolyzed normalized by the estimated amount of SecA available on the mica surface. (**D**) Solution-based assay. Error bars are SEMs and are shown for all data points, although some are not visible because they are smaller than the points.

In addition to area analyses, the height distributions also indicated that SecA-WT was conformationally more dynamic as compared to the SecAΔPBD mutant. Figure 3 (B and D) shows height distributions of SecA-WT and SecAΔPBD, respectively. The full width at half maximum (FWHM) of SecA-WT heights was larger than that of the mutant in all the conditions studied. For example, the FWHM in the presence of ATP was 2.3 nm for SecA-WT compared to 1.5 nm for the SecAΔPBD mutant (green curves in Fig. 3, B and D). This difference can be attributed to the PBD and motions thereof. Differences in conformational dynamics (evinced by FWHM of the height distributions) were pronounced even in the absence of ATP. The FWHM of apo SecA-WT was 50% larger than that of apo SecAΔPBD. Preincubation in ATP, followed by imaging in the absence of ATP (Fig. 3, red), shifted the overall height of SecA downward by ~0.4 nm for both SecA-WT and the SecAΔPBD mutant. When imaged in ATP, this shift was eliminated for SecA-WT, but not for SecAΔPBD. A similar conformational change was reported for a different enzyme (adenylate kinase) when exposed to ATP and was attributed to a partially closed conformational state that would allow rapid product-substrate exchange (*31*). The overall similarity between the three SecA-WT height distributions is notable (Fig. 3B); all conditions showed two principle height peaks and a prominent shoulder at ~5 nm.

To further investigate the conformational changes, we exposed SecA-WT and the SecAΔPBD mutant to two nonhydrolyzable nucleotides: adenosine diphosphate (ADP) and ADP-AlF_3, an ATP analog that conformationally stabilizes or traps the ATPase in its transition state (*32*, *33*). Enzymes were exposed to ADP or ADP-AlF_3 for 15 min before imaging and then imaged in the absence of nucleotides. Representative images of SecA-WT and SecAΔPBD after ADP or ADP-AlF_3 exposure are shown (fig. S8). Footprint area distributions are presented in Fig. 4 [A (SecA-WT) and B (SecAΔPBD)]. SecA-WT footprint areas increased when compared to the apo state: After ADP exposure, the primary peak position was at 220 nm^2 (Fig. 4A, cyan); after ADP-AlF_3 exposure, the primary peak was at 235 nm^2 (Fig. 4A, gray). The magnitudes of these increases were smaller when compared to preincubation in ATP (Fig. 4A, red dashed). In the case of SecAΔPBD, the area distributions remained essentially the same after exposure to ADP or the nonhydrolyzable analog ADP-AlF_3 [primary peak positions: 220 nm^2 (cyan) and 220 nm^2 (gray); Fig. 4B]. This provides further evidence that the corresponding increases in footprint area observed with SecA-WT were due to PBD motion.

Figure 4 (C and E) shows height distributions of SecA-WT after ADP and ADP-AlF_3 exposure, respectively. The height shifted lower than that of the apo state when the WT enzyme was exposed to either of these two nucleotides. The FWHM of these data and the associated statistics are presented in table S4. The height distributions after exposure to the two nonhydrolyzable nucleotides were sharply peaked as compared to the apo state (compare cyan and gray to black dashed; Fig. 4, C and E). Thus, it appears that most of the populations observed upon ADP and ADP-AlF_3 exposure represent nucleotide-stabilized conformational states, similar to those reported previously in bulk studies (*29*). Height histograms acquired with either ADP or ADP-AlF_3 in the imaging buffer (fig. S9) were similar to the nucleotide-exposed conditions. Hence, conformational changes were persistent.

It is informative to compare height distribution shifts for SecA-WT and SecAΔPBD when exposed to the two nonhydrolyzable nucleotides. In the case of the SecAΔPBD mutant, the height distributions for the apo state and the ADP-exposed state were similar (Fig. 4D). In contrast, for the WT species, the ADP-exposed state was altered significantly from the apo state, exhibiting a single sharp peak compared to a bimodal apo peak (Fig. 4C). These results imply that ADP induces a conformational state change in the PBD.

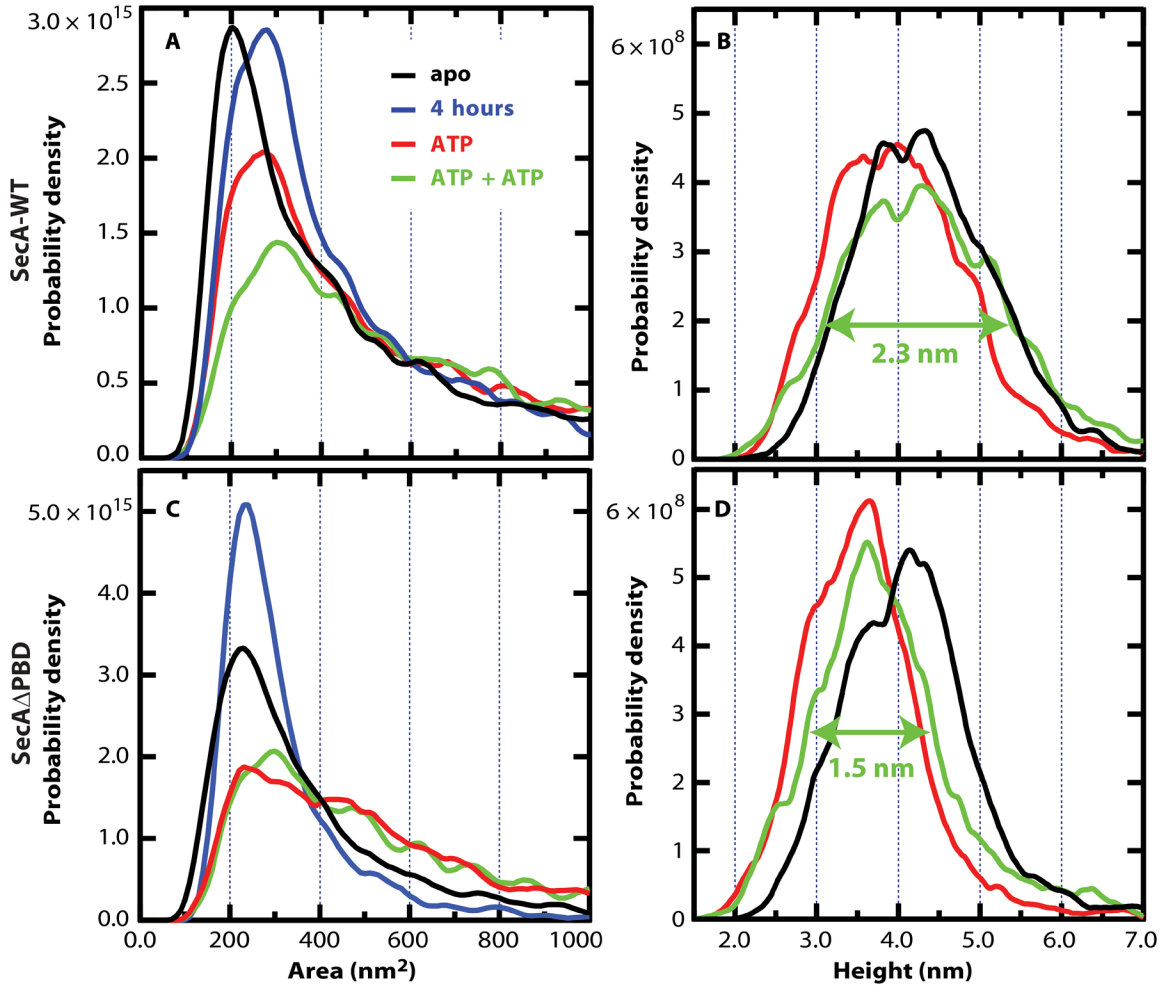

Fig. 3. Role of the PBD in SecA dynamics. (**A**) Distribution of footprint area for SecA-WT in different conditions: (i) apo: black, $n = 3726$; (ii) ATP: red, 15-min preincubation in ATP and imaged in the absence of ATP, $n = 3376$; (iii) ATP + ATP: green, 15-min preincubation in ATP and imaged in presence of ATP, $n = 2437$; and (iv) 4 hours: blue, 4 hours after exposure to ATP and imaged in the absence of ATP, $n = 2448$. (**B**) Distribution of SecA-WT heights in differing nucleotide conditions [color codes carry over from (A)]. (**C**) Footprint area and (**D**) height distributions for SecAΔPBD (apo, $n = 4009$; ATP, $n = 1907$; ATP + ATP, $n = 1458$; 4 hours, $n = 1061$). Note that, in ATP, the FWHM of the SecAΔPBD mutant height distribution is 65% smaller than the WT.

The results with the transition state analog provide additional insight into the conformational dynamics. For the SecAΔPBD mutant, the ADP-ALF_3– and ATP-exposed states exhibited similar height distributions (Fig. 4F, gray and red dashed, respectively), and both nucleotides shifted the overall heights lower compared to the apo state. Analogous behavior was observed for the SecA-WT species (Fig. 4E). The shifts from the apo state to the ADP-AlF_3 state were similar in magnitude for SecA-WT and SecAΔPBD and suggestive of a common underlying origin. It thus appears that ADP-AlF_3 binding induces a conformational change, likely in the C-terminal segment of SecA, that manifests as a height change in the AFM measurements. Area analysis showed ADP-AlF_3–induced shifts for SecA-WT, but not for SecAΔPBD. We conclude that the area shift results from PBD motion, as this is only seen in the WT enzyme, whereas the height shift is common to both species and is likely due to the C-terminal segment. Together, these data indicate a concomitant conformational change: both the PBD and likely the C-terminal segment move upon ADP-AlF_3 exposure.

Imaging SecA after exposure to nonhydrolyzable nucleotides indicated that most of the molecules become stalled in "locked" states, but switching between states is of fundamental importance for hydrolysis. Hence, we followed individual SecA-WT molecules in real time and directly visualized conformational dynamics during ATP hydrolysis. To better observe conformational dynamics, we enhanced the temporal resolution to ~100 ms by repeatedly scanning in one dimension to generate kymographs. First, a traditional two-dimensional image was taken to identify a protein of interest (Fig. 5A). Then, the slow scan axis was disabled to repeatedly scan over the same protein to monitor conformational dynamics under physiological conditions in the absence of ATP (Fig. 5B). We then exploited the large difference evident in the protein area footprint distributions (shown in Fig. 3A) to monitor real-time dynamics as the substrate ATP was consumed.

Kymographs during ATP hydrolysis revealed at least two distinct conformational states exhibiting different width profiles that interconverted back and forth over time (Fig. 5C; see also line scans in Fig. 5D, which are separated by ~100 ms). This apparent conformational

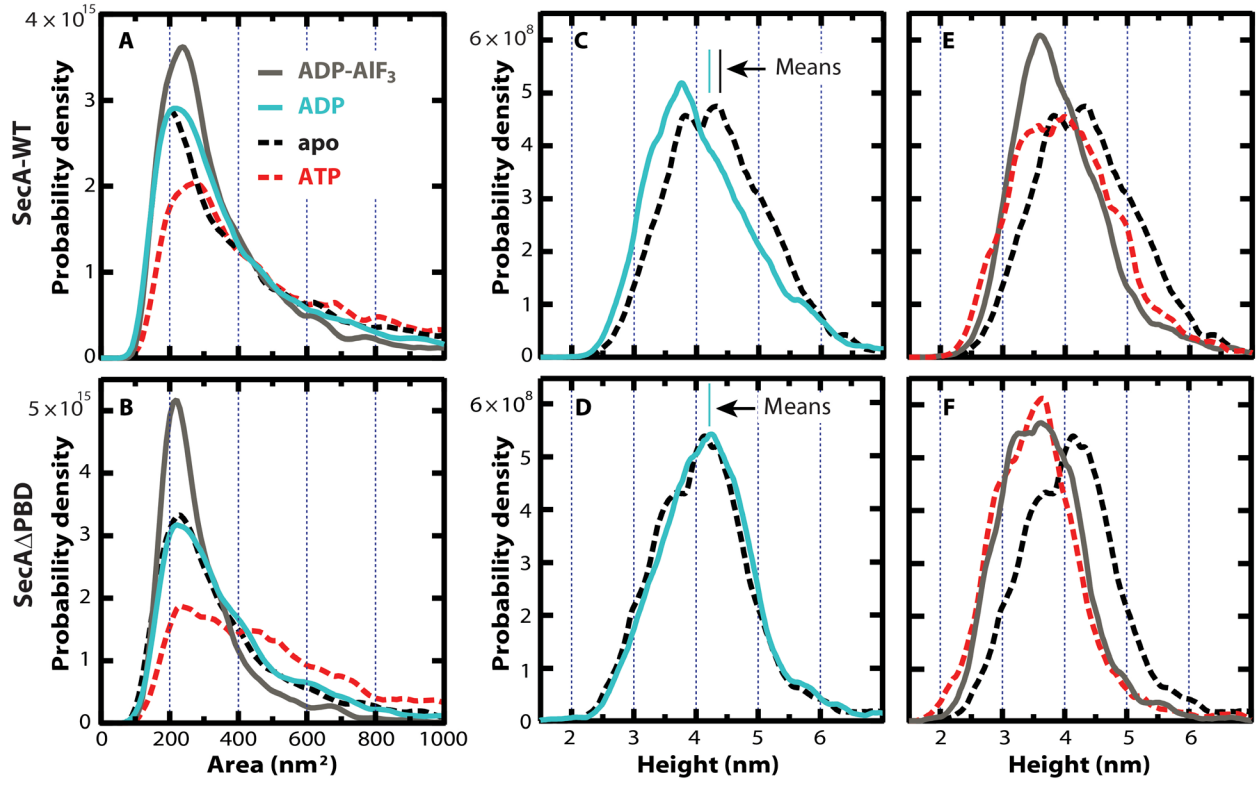

Fig. 4. Nucleotide-stabilized conformations. (**A** and **B**) Area footprint distributions are shown for SecA-WT and SecAΔPBD, respectively. Corresponding height distributions for (**C** and **E**) SecA-WT and (**D** and **F**) SecAΔPBD are shown. Color codes indicate different conditions: cyan, preincubated with ADP (SecA-WT, $n = 6428$; SecAΔPBD, $n = 3104$); gray, preincubated with ADP-AlF$_3$ (SecA-WT, $n = 4590$; SecAΔPBD, $n = 2159$); red dashed, preincubated with ATP; black dashed, apo. Dashed data carried over from Fig.3 for reference. Preincubations were carried out for 15 min in solution, and imaging was performed in the absence of nucleotides in the buffer. Vertical lines in (**C**) and (**D**) show arithmetic means, and the width of the lines is the SEM. Note that only the ADP mean is visible in (D) because the means are identical to within uncertainty (0.2 Å). Additional statistical information is provided for all datasets (tables S1 to S4).

"flickering" was captured over extended periods, illustrating the reversible nature of the dynamics.

Figure 5E illustrates a kymograph of SecA-WT in the presence of ATP over more than 75 s. Here, the protein interconverted between a "compact" and an "extended" state. The green trace in Fig. 5F shows the full width distribution profile of this molecule for the same period of time. The reversible switching of the molecule between compact and extended states is reflected in the histogram as two populations, which are separated by a minimum, positioned at ~29 nm. Additional kymograph data are presented (fig. S10). The data exhibit at least two conformational states, despite differing scan trajectories with respect to the adsorbed protein. Note that all width measurements are overestimates of true molecular dimensions due to tip convolution (nominal tip radius, ~8 nm). During ATP hydrolysis (i.e., with ATP present), the protein favored the extended state over the compact state. Specifically, it remained in the extended state for 84% of the time and 14% in the compact state. We note that the rate-limiting step of the SecA ATP hydrolysis cycle is ADP release. Hence, the prominent extended state is likely to represent the ADP-bound posthydrolysis state of SecA.

DISCUSSION

Single-molecule AFM studies of enzymes undergoing catalysis have been challenging, as many molecules can remain inactive during studies (*34*). In this work, we measured the biochemical activity of surface-adsorbed SecA prepared for AFM study. Tracking the release of Pi verified ATP hydrolysis over timescales commensurate with AFM imaging and suggested that a significant fraction of SecA was undergoing ATP hydrolysis at a similar rate to that measured in solution. With the assurance that SecA retained ATPase activity when adsorbed to mica, we applied AFM to capture conformations and conformational dynamics associated with ATP hydrolysis.

The height distribution for individual SecA-WT molecules in the apo state exhibited a maximum at around 4 nm, in overall agreement with previously reported distributions for SecA when bound to SecYEG in membrane using the same technique (*7*, *21*). To aid interpretation, we generated simulated AFM images of SecA monomers using crystal structure coordinates and an assumed tip geometry based on the manufacturer's nominal dimensions. Simulated images (fig. S2) were in overall agreement with the experimental data.

Exposing SecA-WT to ATP increased the areal footprint of the enzyme significantly and did so over long timescales (~4 hours). What is the origin of these long-lived ATP-dependent conformational changes? Structures have suggested that the PBD undergoes a large-scale swivel motion (approximately 80°; Fig. 1B) (*1*). But, it is important to note that, in the x-ray structures of SecA from *E. coli* (PDB code: 2FSF), the PBD region is not resolved. This is likely an indication that the PBD populates diverse conformations without having one state significantly more stable than the others. However,

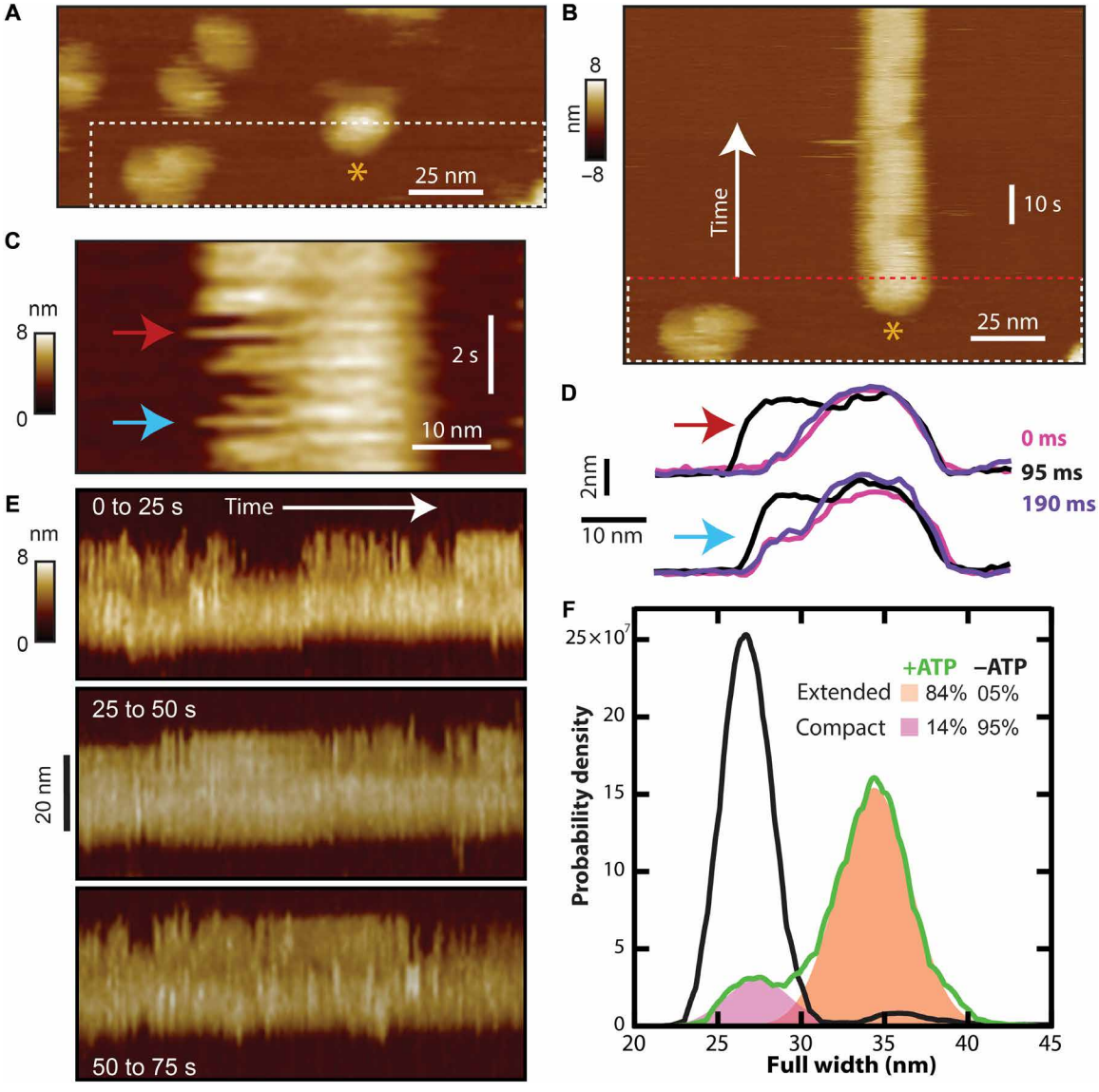

Fig. 5. Reversible conformational dynamics of individual SecA during ATP hydrolysis. (**A**) AFM image of SecA-WT in the absence of ATP, white dashed rectangle shows area for detailed study, and asterisk identifies molecule of interest. (**B**) Upon rescanning and identifying the same molecule, a kymograph is instigated: the time axis begins at the top of the area (red dashed line). (**C**) Detailed view of kymograph in the presence of ATP. (**D**) Sequential height profiles separated by 95 ms (temporal sequence: pink, black, and purple) corresponding to arrows in (C). (**E**) Kymograph of SecA with ATP over 75 s and (**F**) histogram of AFM-measured SecA full width (number of scan lines, $n = 406$) showing two subpopulations: compact and extended.

these dynamics have proven challenging to observe. Nuclear magnetic resonance (NMR) studies on full-length SecA have provided limited information (*9*, *35*). Molecular dynamics simulation results have suggested that the transition from open to closed state occurs in two distinct phases. Initially, the PBD and the C-terminal region move as a single unit, and then the PBD moves alone in the second phase, toward NBD2 to the fully closed state (*17*). AFM imaging indicated that the PBD explored a much wider conformational space when SecA was exposed to ATP compared to the apo state and provided evidence of PBD motion as well as PBD motion coupled with motion of other protein segments occurring in a nucleotide-dependent manner.

ADP binding shifted both the area and height distributions for SecA-WT but did not alter the corresponding distributions for SecAΔPBD. Hence, ADP binding directly affected the PBD conformation. Furthermore, binding of ADP-AlF_3, the nonhydrolyzable ATP analog that traps SecA in its transition state, shifted the height peak for both SecA-WT and the SecAΔPBD mutant to similar values. This suggested a change in conformation of the C-terminal segment, a common element that is thought to dock onto SecY at the membrane interface and regulate ATPase activity (*1*, *9*, *17*). We note that we cannot rule out the possibility that the NBD1 and NBD2 domains, which are also common to SecA-WT and SecAΔPBD, could also be responsible for observed motion. The ADP-AlF_3–induced height shift was accompanied by an area shift for the WT enzyme, but not for the mutant. Together, the data imply that the transition state of the system involves conformational displacements of both

the PBD and likely the C-terminal segment and that the resting state of the system (ADP-bound) is characterized by a change of just the PBD with respect to the remainder of the protein. These results are consistent with NMR studies on SecA derivatives and biochemical studies. It has been proposed that ATP binding and hydrolysis lead to a shift in equilibrium between disorder and order of the nucleotide binding cleft, and this shift is allosterically propagated to the PBD through the HSD in the C-terminal segment (*9*, *29*, *36*).

We followed individual SecA molecules in real time in an attempt to directly visualize conformational dynamics associated with ATP hydrolysis. To more readily observe these dynamics, we enhanced the temporal resolution by raster scanning in one spatial dimension rather than two. The resulting kymographs revealed two distinct conformational states of SecA: extended and compact.

ATP hydrolysis is known to consist of multiple steps: (i) ATP binding to SecA; (ii) ATP conversion to ADP and Pi; (iii) Pi release; and (iv) ADP release. So why do we observe only two states? ATP is rapidly hydrolyzed to ADP upon binding (*37*), and Pi release is rapid and not rate-limiting (*38*). In contrast, ADP release is known to be slow and rate-limiting (*29*, *38*–*40*). Previous biochemical assays revealed that the SecA ATP catalytic cycle consists of two distinct events (*29*, *41*). ATP exposure led to a significant (1.5-fold; Fig. 3A) increase in footprint area, which can be related to the extended state (more area = more width). Because the extended state was the dominant state in the kymographs with ATP, we propose that this state represents the ADP-bound posthydrolysis state, whereas the compact state represents one or more of steps (i) to (iii), which occur too rapidly to be resolved in our AFM measurements.

The conformational change from the compact state to extended state observed in the kymographs can be associated with ATP binding and hydrolysis. A conformational change is required for ADP release, and ADP release is the rate-limiting step (*29*). Hence, the conformational change from the dominant extended state to the compact state is likely associated with ADP release. This is supported by the observation that the apo state was compact: it exhibited the smallest area we observed. Previous studies have shown that only hydrolyzable ATP can drive processive preprotein translocation but not ADP or other nonhydrolyzable ATP analogs (*12*, *42*). Further, the PBD is known to be in direct contact with precursor proteins (*1*, *3*, *4*). Therefore, the two dominant states observed in the kymographs are likely associated with translocation.

We studied conformational dynamics during basal SecA-ATP hydrolysis. Our measurements were carried out in real time and real space via single-molecule AFM imaging. We showed that SecA undergoes reversible conformational changes in the presence of ATP and that the proteins can be stalled in locked states upon exposure to nonhydrolyzable ATP analogs. Evidence of nucleotide-dependent motion of the PBD alone, and the PBD in conjunction with other segments of the protein, was provided. More generally, we demonstrate here a capability of AFM to study reversible conformational dynamics at the single-molecule level for the characterization of ligand-induced changes in SecA.

MATERIALS AND METHODS

Protein purification

SecA-WT was purified following standard protocols described in reference (*7*). The SecAΔPBD mutant (amino acids 231 to 369 deleted) is SecAC4 [a SecA variant that lacks zinc because the coordinating cysteines have been replaced by serine (*26*)] engineered to remove the protein-binding domain. The construct was made commercially (Mutagenex Inc.), and the protein was purified as described (*7*).

ATPase activity assay

To mimic the sample preparation for AFM measurements, SecA was preincubated for 15 min at 2.4 μM (25°C) in adsorption solution: 10 mM Hepes (pH 7.6), 100 mM KAc, 5 mM $MgAc_2$, and 3 mM ATP. One hundred microliters of this solution was deposited onto freshly cleaved mica (Ted Pella) and incubated for 15 min at 25°C. The sample was rinsed 10 times with 100 μl of adsorption solution to remove unbound SecA. Then, 50 μl of the adsorption solution was replaced with 50 μl of solution containing radiolabeled ATP: 10 mM Hepes (pH 7.6), 100 mM KAc, 5 mM $MgAc_2$, 3 mM ATP, 3.3 mM [γ-^{32}P]ATP (0.908 nCi/μl; PerkinElmer). At corresponding times, 2 μl was removed to tubes with 50 mM EDTA to stop the hydrolysis reaction and applied to a thin-layer chromatography plate (Millipore Corporation). After application of all samples, the plate was developed in 125 mM KH_2PO_4. After drying, the plates were exposed and scanned using a PhosphorImager. The percentage of ATP hydrolyzed was estimated from the proportion of total radioactivity that migrated as Pi. To evaluate ATPase activity in solution, the aforementioned procedure was carried out in the absence of the mica incubation and rinsing steps.

Sample preparation for AFM

SecA was diluted to 20 nM and incubated for 15 min in one of two solutions: (i) no substrate (apo) conditions [10 mM Hepes (pH 7.6), 100 mM KAc, and 5 mM $MgAc_2$] or (ii) saturating nucleotide (ATP, ADP, or ADP-AlF_3) conditions [10 mM Hepes (pH 7.6), 100 mM KAc, 5 mM $MgAc_2$, and 100 μM nucleotide]. One hundred fifty microliters of this solution was then deposited onto a freshly cleaved mica surface. After 10-min incubation on mica, the sample was rinsed 10 times with 100 μl of the appropriate solution.

Atomic force microscopy

AFM images were acquired at ~32°C in tapping mode using a commercial instrument (Asylum Research Cypher) in 10 mM Hepes (pH 7.6), 100 mM KAc, and 5 mM $MgAc_2$ or 10 mM Hepes (pH 7.6), 100 mM KAc, 5 mM $MgAc_2$,and 100 μM nucleotide, as specified. Measurement-related bias of protein conformations and conformational dynamics is an ever present concern. Care was taken to control the magnitude of the tip sample force to $\lesssim$100 pN [estimated by comparing the free amplitude (~10 nm) to the set point amplitude]. BioLever mini tips (BL-AC40TS, Olympus) with measured spring constants of ~0.06 N/m were used. Spring constants were determined using the thermal noise method. AFM images were acquired with the following parameters: scan rate, 3.6 Hz; scan size, 512 pixels × 512 pixels, 1 μm^2 × 1 μm^2; scan speed, 7 nm/ms. Kymographs were acquired as follows: scan rate, 5.2 Hz; scan size, 320 pixels, 300 nm; scan speed, 3 nm/ms. We analyzed at least 17 images per condition studied, at least 3 independent experiments/mica stages/sample preparations per condition, and at least 2 different tips for each independent experiment. Note that tips were recovered after each experiment and cleaned for reuse.

Data analysis

Individual SecA molecules were identified and extracted from large-scale AFM images via the Hessian blob algorithm implemented in custom software (Igor Pro 7; Wavemetrics, Portland, OR) (*22*). A local

background level was determined for each individual molecule via Laplace interpolation, providing an accurate baseline from which various molecule metrics were measured. The molecule height was defined as the largest height above the local background level obtained within the molecule. We defined the footprint area as the area occupied by the molecule projected into the flat *XY* plane, computed as the number of pixels within the molecule scaled by the area per pixel. For kymograph width distribution histograms, line scan traces were analyzed manually. Gaussian fitting was performed using MagicPlot.

Simulations of AFM images and related analysis

Simulated AFM images were produced (fig. S2) by modeling the interaction between a SecA molecule and the AFM tip during the imaging process. The action of "scanning" the AFM tip across a sample surface to produce an image was captured mathematically by the morphological dilation operation, which is responsible for the convolution effect seen in AFM imagery by tips that are not perfectly sharp. To construct a simulated AFM image of SecA, we explicitly computed the morphological dilation between three-dimensional models of SecA and an AFM tip. SecA was modeled via its x-ray crystal structure where each atom was modeled as a sphere with the van der Waals radius (*43*). The AFM tip was modeled as a cone with a rounded, spherical tip using nominal specifications from the manufacturer (cone angle, 17.5°; tip radius, 8 nm). A simulated AFM image was then produced using custom software (Igor Pro 7; Wavemetrics, Portland, OR). To compare simulated and experimental images (fig. S3), the residual between the images was squared and integrated, with the square root of the result then used to quantify the discrepancy between the images. The discrepancy was normalized as a percentage of the total volume of the experimental image. We then defined the percent agreement as one minus the normalized discrepancy. The agreement was maximized over all relative orientations (translations and rotations) between the experimental and simulated images. To generate equipotential surface maps (fig. S5), electrostatic potentials were calculated with the APBS software (*44*) at pH 7.

SUPPLEMENTARY MATERIALS

Supplementary material for this article is available at http://advances.sciencemag.org/cgi/content/full/4/10/eaat8797/DC1

Fig. S1. Tapping mode phase imaging.
Fig. S2. Simulated AFM images and likely orientations of SecA on surface.
Fig. S3. AFM image data corroborate with simulations.
Fig. S4. Statistically robust subpopulations.
Fig. S5. Equipotential surfaces comparing the front and back faces of SecA.
Fig. S6. Evaluation of molecular density of SecA prepared for surface-adsorbed ATPase activity assays.
Fig. S7. Representative images of SecA-WT and SecAΔPBD subject to different conditions.
Fig. S8. Representative images of SecA-WT and SecAΔPBD exposed to different nucleotides.
Fig. S9. Height histograms of SecA immersed in and exposed to nonhydrolyzable nucleotides.
Fig. S10. Additional kymograph data.
Table S1. Statistics of SecA-WT (WT) and SecAΔPBD (ΔPBD) area distributions in the following conditions.
Table S2. Mean height (±SEM) and FWHM of the SecA-WT and the SecAΔPBD mutant height distributions in different conditions.
Table S3. Statistics of the SecA-WT and SecAΔPBD area distributions after exposure to ADP or ADP-AlF_3.
Table S4. Mean height (±SEM) and FWHM of the SecA-WT and the SecAΔPBD mutant distributions exposed to ADP and ADP-AlF_3.

REFERENCES AND NOTES

1. A. Tsirigotaki, J. De Geyter, N. Šoštaric, A. Economou, S. Karamanou, Protein export through the bacterial Sec pathway. *Nat. Rev. Microbiol.* **15**, 21–36 (2017).
2. J. M. Crane, L. L. Randall, The Sec system: Protein export in *Escherichia coli*. *EcoSal Plus* **7**, 10.1128/ecosalplus.ESP-0002-2017 (2017).
3. W. J. Allen, R. A. Corey, P. Oatley, R. B. Sessions, S. A. Baldwin, S. E. Radford, R. Tuma, I. Collinson, Two-way communication between SecY and SecA suggests a Brownian ratchet mechanism for protein translocation. *eLife* **5**, e15598 (2016).
4. B. W. Bauer, T. Shemesh, Y. Chen, T. A. Rapoport, A "push and slide" mechanism allows sequence-insensitive translocation of secretory proteins by the SecA ATPase. *Cell* **157**, 1416–1429 (2014).
5. K. Cunningham, R. Lill, E. Crooke, M. Rice, K. Moore, W. Wickner, D. Oliver, SecA protein, a peripheral protein of the Escherichia coli plasma membrane, is essential for the functional binding and translocation of proOmpA. *EMBO J.* **8**, 955–959 (1989).
6. K. Dalal, C. S. Chan, S. G. Sligar, F. Duong, Two copies of the SecY channel and acidic lipids are necessary to activate the SecA translocation ATPase. *Proc. Natl. Acad. Sci. U.S.A.* **109**, 4104–4109 (2012).
7. C. Mao, C. E. Cheadle, S. J. Hardy, A. A. Lilly, Y. Suo, R. R. Sanganna Gari, G. M. King, L. L. Randall, Stoichiometry of SecYEG in the active translocase of *Escherichia coli* varies with precursor species. *Proc. Natl. Acad. Sci. U.S.A.* **110**, 11815–11820 (2013).
8. T. R. Matin, K. P. Sigdel, M. Utjesanovic, B. P. Marsh, F. Gallazzi, V. F. Smith, I. Kosztin, G. M. King, Single-molecule peptide–lipid affinity assay reveals interplay between solution structure and partitioning. *Langmuir* **33**, 4057–4065 (2017).
9. D. Keramisanou, N. Biris, I. Gelis, G. Sianidis, S. Karamanou, A. Economou, C. G. Kalodimos, Disorder-order folding transitions underlie catalysis in the helicase motor of SecA. *Nat. Struct. Mol. Biol.* **13**, 594– 602 (2006).
10. J. Zimmer, Y. Nam, T. A. Rapoport, Structure of a complex of the ATPase SecA and the protein-translocation channel. *Nature* **455**, 936–943 (2008).
11. G. Gouridis, S. Karamanou, M. F. Sardis, M. A. Schärer, G. Capitani, A. Economou, Quaternary dynamics of the SecA motor drive translocase catalysis. *Mol. Cell* **52**, 655–666 (2013).
12. E. Schiebel, A. J. M. Driessen, F.-U. Hartl, W. Wickner, $\Delta\mu_H$+ and ATP function at different steps of the catalytic cycle of preprotein translocase. *Cell* **64**, 927–939 (1991).
13. F.-C. Liang, U. K. Bageshwar, S. M. Musser, Bacterial Sec protein transport is rate-limited by precursor length: A single turnover study. *Mol. Biol. Cell* **20**, 4256–4266 (2009).
14. J. F. Hunt, S. Weinkauf, L. Henry, J. J. Fak, P. McNicholas, D. B. Oliver, J. Deisenhofer, Nucleotide control of interdomain interactions in the conformational reaction cycle of SecA. *Science* **297**, 2018–2026 (2002).
15. E. Park, T. A. Rapoport, Mechanisms of Sec61/SecY-mediated protein translocation across membranes. *Annu. Rev. Biophys.* **41**, 21–40 (2012).
16. A. R. Osborne, W. M. Clemons Jr., T. A. Rapoport, A large conformational change of the translocation ATPase SecA. *Proc. Natl. Acad. Sci. U.S.A.* **101**, 10937–10942 (2004).
17. Y. Chen, B. W. Bauer, T. A. Rapoport, J. C. Gumbart, Conformational changes of the clamp of the protein translocation ATPase SecA. *J. Mol. Biol.* **427**, 2348–2359 (2015).
18. D. J. Muller, Y. F. Dufrêne, Atomic force microscopy as a multifunctional molecular toolbox in nanobiotechnology. *Nat. Nanotechnol.* **3**, 261–269 (2008).
19. T. Ando, T. Uchihashi, S. Scheuring, Filming biomolecular processes by high-speed atomic force microscopy. *Chem. Rev.* **114**, 3120–3188 (2014).
20. R. R. Sanganna Gari, N. C. Frey, C. Mao, L. L. Randall, G. M. King, Dynamic structure of the translocon SecYEG in membrane: Direct single molecule observations. *J. Biol. Chem.* **288**, 16848–16854 (2013).
21. N. Chada, K. P. Sigdel, R. R. Gari, T. R. Matin, L. L. Randall, G. M. King, Glass is a viable substrate for precision force microscopy of membrane proteins. *Sci. Rep.* **5**, 12550 (2015).
22. B. P. Marsh, N. Chada, R. R. Sanganna Gari, K. P. Sigdel, G. M. King, The Hessian blob algorithm: Precise particle detection in atomic force microscopy imagery. *Sci. Rep.* **8**, 978 (2018).
23. R. L. Woodbury, S. J. S. Hardy, L. L. Randall, Complex behavior in solution of homodimeric SecA. *Protein Sci.* **11**, 875–882 (2002).
24. S. N. Magonov, V. Elings, M.-H. Whangbo, Phase imaging and stiffness in tapping-mode atomic force microscopy. *Surf. Sci.* **375**, L385–L391 (1997).
25. D. J. Müller, D. Fotiadis, S. Scheuring, S. A. Müller, A. Engel, Electrostatically balanced subnanometer imaging of biological specimens by atomic force microscope. *Biophys. J.* **76**, 1101–1111 (1999).
26. C. Mao, S. J. S. Hardy, L. L. Randall, Maximal efficiency of coupling between ATP hydrolysis and translocation of polypeptides mediated by SecB requires two protomers of SecA. *J. Bacteriol.* **191**, 978–984 (2009).
27. L. B. Jilaveanu, C. R. Zito, D. Oliver, Dimeric SecA is essential for protein translocation. *Proc. Natl. Acad. Sci. U.S.A.* **102**, 7511–7516 (2005).
28. J. L. Maki, B. Krishnan, L. M. Gierasch, Using a low denaturant model to explore the conformational features of translocation-active SecA. *Biochemistry* **51**, 1369–1379 (2012).
29. J. J. Fak, A. Itkin, D. D. Ciobanu, E. C. Lin, X. J. Song, Y. T. Chou, L. M. Gierasch, J. F. Hunt, Nucleotide exchange from the high-affinity ATP-binding site in SecA is the rate-limiting step in the ATPase cycle of the soluble enzyme and occurs through a specialized conformational state. *Biochemistry* **43**, 7307–7327 (2004).
30. E. Papanikou, S. Karamanou, C. Baud, M. Frank, G. Sianidis, D. Keramisanou, C. G. Kalodimos, A. Kuhn, A. Economou, Identification of the preprotein binding domain of SecA. *J. Biol. Chem.* **280**, 43209–43217 (2005).

31. B. Pelz, G. Žoldák, F. Zeller, M. Zacharias, M. Rief, Subnanometre enzyme mechanics probed by single-molecule force spectroscopy. *Nat. Commun.* **7**, 10848 (2016).
32. K. J. Erlandson, E. Or, A. R. Osborne, T. A. Rapoport, Analysis of polypeptide movement in the SecY channel during SecA-mediated protein translocation. *J. Biol. Chem.* **283**, 15709–15715 (2008).
33. B. Chen, M. Doucleff, D. E. Wemmer, S. De Carlo, H. H. Huang, E. Nogales, T. R. Hoover, E. Kondrashkina, L. Guo, B. T. Nixon, ATP ground- and transition-states of bacterial enhancer binding AAA+ ATPases support complex formation with their target protein, σ54. *Structure* **15**, 429–440 (2007).
34. Y. Ruan, A. Miyagi, X. Wang, M. Chami, O. Boudker, S. Scheuring, Direct visualization of glutamate transporter elevator mechanism by high-speed AFM. *Proc. Natl. Acad. Sci. U.S.A.* **114**, 1584–1588 (2017).
35. Y.-T. Chou, J. F. Swain, L. M. Gierasch, Functionally significant mobile regions of *Escherichia coli* SecA ATPase identified by NMR. *J. Biol. Chem.* **277**, 50985–50990 (2002).
36. H. Mori, K. Ito, The long α-helix of SecA is important for the ATPase coupling of translocation. *J. Biol. Chem.* **281**, 36249–36256 (2006).
37. M. Schmidt, H. Ding, V. Ramamurthy, I. Mukerji, D. Oliver, Nucleotide binding activity of SecA homodimer is conformationally regulated by temperature and altered by *prlD* and *azi* mutations. *J. Biol. Chem.* **275**, 15440–15448 (2000).
38. A. Robson, V. A. M. Gold, S. Hodson, A. R. Clarke, I. Collinson, Energy transduction in protein transport and the ATP hydrolytic cycle of SecA. *Proc. Natl. Acad. Sci. U.S.A.* **106**, 5111–5116 (2009).
39. C. R. Zito, E. Antony, J. F. Hunt, D. B. Oliver, M. M. Hingorani, Role of a conserved glutamate residue in the *Escherichia coli* SecA ATPase mechanism. *J. Biol. Chem.* **280**, 14611–14619 (2005).
40. G. Sianidis, S. Karamanou, E. Vrontou, K. Boulias, K. Repanas, N. Kyrpides, A. S. Politou, A. Economou, Cross-talk between catalytic and regulatory elements in a DEAD motor domain is essential for SecA function. *EMBO J.* **20**, 961–970 (2001).
41. J. P. W. van der Wolk, J. G. de Wit, A. J. M. Driessen, The catalytic cycle of the *Escherichia coli* SecA ATPase comprises two distinct preprotein translocation events. *EMBO J.* **16**, 7297–7304 (1997).
42. J. de Keyzer, C. van der Does, T. G. Kloosterman, A. J. M. Driessen, Direct demonstration of ATP-dependent release of SecA from a translocating preprotein by surface plasmon resonance. *J. Biol. Chem.* **278**, 29581–29586 (2003).
43. S. Alvarez, A cartography of the van der Waals territories. *Dalton Trans.* **42**, 8617–8636 (2013).
44. E. Jurrus, D. Engel, K. Star, K. Monson, J. Brandi, L. E. Felberg, D. H. Brookes, L. Wilson, J. Chen, K. Liles, M. Chun, P. Li, D. W. Gohara, T. Dolinsky, R. Konecny, D. R. Koes, J. E. Nielsen, T. Head-Gordon, W. Geng, R. Krasny, G. W. Wei, M. J. Holst, J. A. McCammon, N. A. Baker, Improvements to the APBS biomolecular solvation software suite. *Protein Sci.* **27**, 112–128 (2018).

Acknowledgments: We are grateful to A. Lilly and Y. Suo for protein purification and quantification. In addition, we wish to thank T. R. Matin, K. P. Sigdel, S. J. S. Hardy, and L. L. Randall for discussions. **Funding:** This work was supported by the National Science Foundation (CAREER award number 1054832 to G.M.K.) and a Burroughs Wellcome Fund Career Award at the Scientific Interface (to G.M.K.). **Author contributions:** N.C. performed AFM experiments and analysis. B.P.M. developed analysis tools and performed analysis. K.C., C.M., P.B., and G.M.K. performed ATPase measurements. All authors contributed to the writing of the manuscript. **Competing interests:** The authors declare that they have no competing interests. **Data and materials availability:** All data needed to evaluate the conclusions in the paper are present in the paper and/or the Supplementary Materials. Additional data related to this paper may be requested from the authors.

Submitted 13 April 2018
Accepted 13 September 2018
Published 24 October 2018
10.1126/sciadv.aat8797

Citation: N. Chada, K. Chattrakun, B. P. Marsh, C. Mao, P. Bariya, G. M. King, Single-molecule observation of nucleotide induced conformational changes in basal SecA-ATP hydrolysis. *Sci. Adv.* **4**, eaat8797 (2018).

ScienceAdvances

Single-molecule observation of nucleotide induced conformational changes in basal SecA-ATP hydrolysis

Nagaraju Chada, Kanokporn Chattrakun, Brendan P. Marsh, Chunfeng Mao, Priya Bariya and Gavin M. King

Sci Adv **4** (10), eaat8797.
DOI: 10.1126/sciadv.aat8797

Science Advances
AAAS

advances.sciencemag.org/cgi/content/full/4/10/eaat8797/DC1

Supplementary Materials for

Single-molecule observation of nucleotide induced conformational changes in basal SecA-ATP hydrolysis

Nagaraju Chada, Kanokporn Chattrakun, Brendan P. Marsh, Chunfeng Mao, Priya Bariya, Gavin M. King*

*Corresponding author. Email: kinggm@missouri.edu

Published 24 October 2018, *Sci. Adv.* **4**, eaat8797 (2018)
DOI: 10.1126/sciadv.aat8797

This PDF file includes:

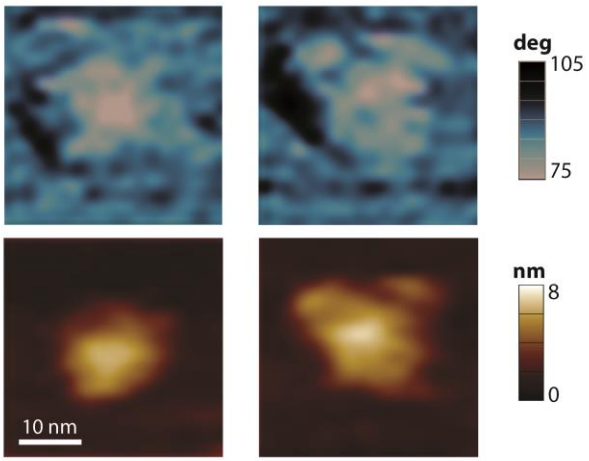

Fig. S1. Tapping mode phase imaging. Tapping mode phase images of SecA-WT are shown above the corresponding topographic images (data from Fig. 1F & G). Phase contrast is generally attributable to local changes in viscoelastic properties of the sample.

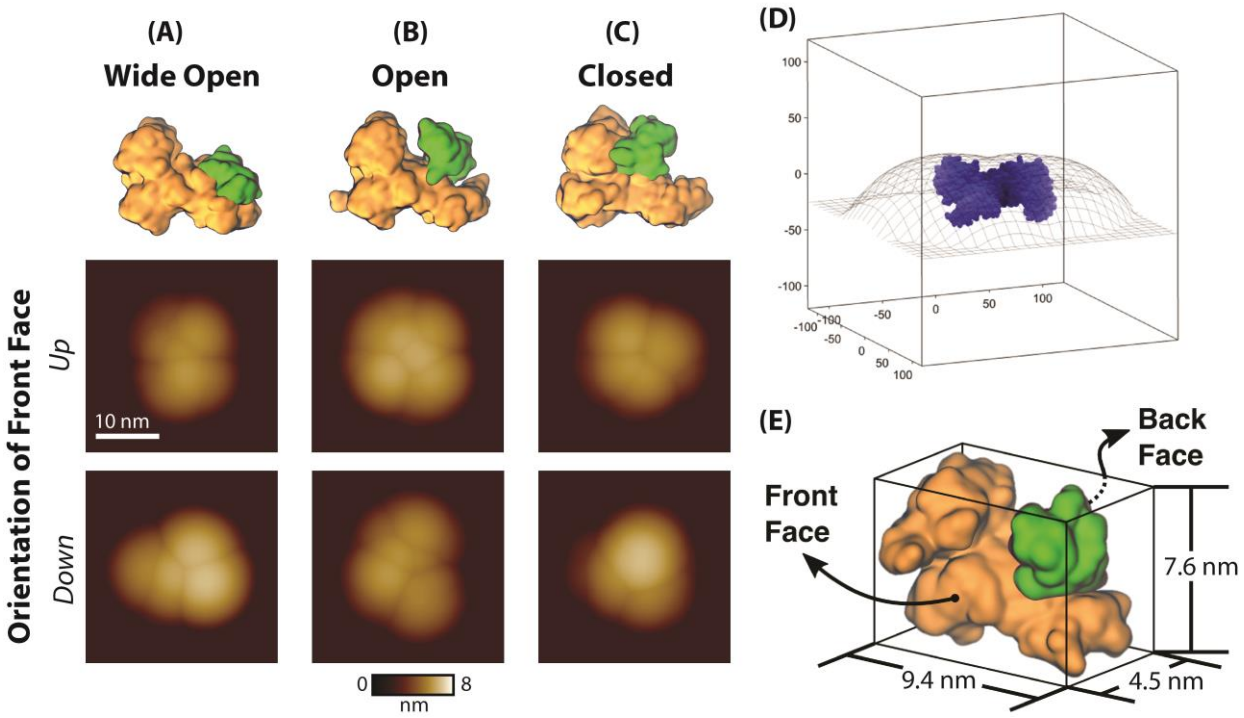

Fig. S2. Simulated AFM images and likely orientations of SecA on surface. Simulated AFM images were constructed from crystal structures and manufacturer nominal tip geometry (BL-AC40TS, Olympus; cone angle = 17.5°, tip radius = 8 nm). Column (**A**): PDB code 1M6N; (**B**): 1TF5; and (**C**): 3DIN. The protein binding domain is drawn in green. (**D**) Shows an example of the convoluted topographical surface (wire mesh) produced by morphological dilation. The protein is drawn in blue in this panel, the units are Å. (**E**) A rectangular volume with SecA inscribed defines two important faces of the molecule, the front and back face. We define the "up" orientation such that the front face of the molecule is in contact with the AFM tip. The "down" orientation is rotated by 180°, such that the front face of the molecule is in contact with the mica surface. We note that all of the experimental data exhibited prominent height peaks around 4.5 nm, consistent with either of these two orientations. All other orientations, without the large front or back face flush with the mica surface, would likely demonstrate height peaks >7 nm. However, significant sub-populations above 6 nm in height were not observed in the experimental data, suggesting a preference towards the up or down orientations. Hence, we focused our analysis on these two orientations. We note that in both the up and down orientation, the AFM tip can directly access and probe protein binding domain dynamics.

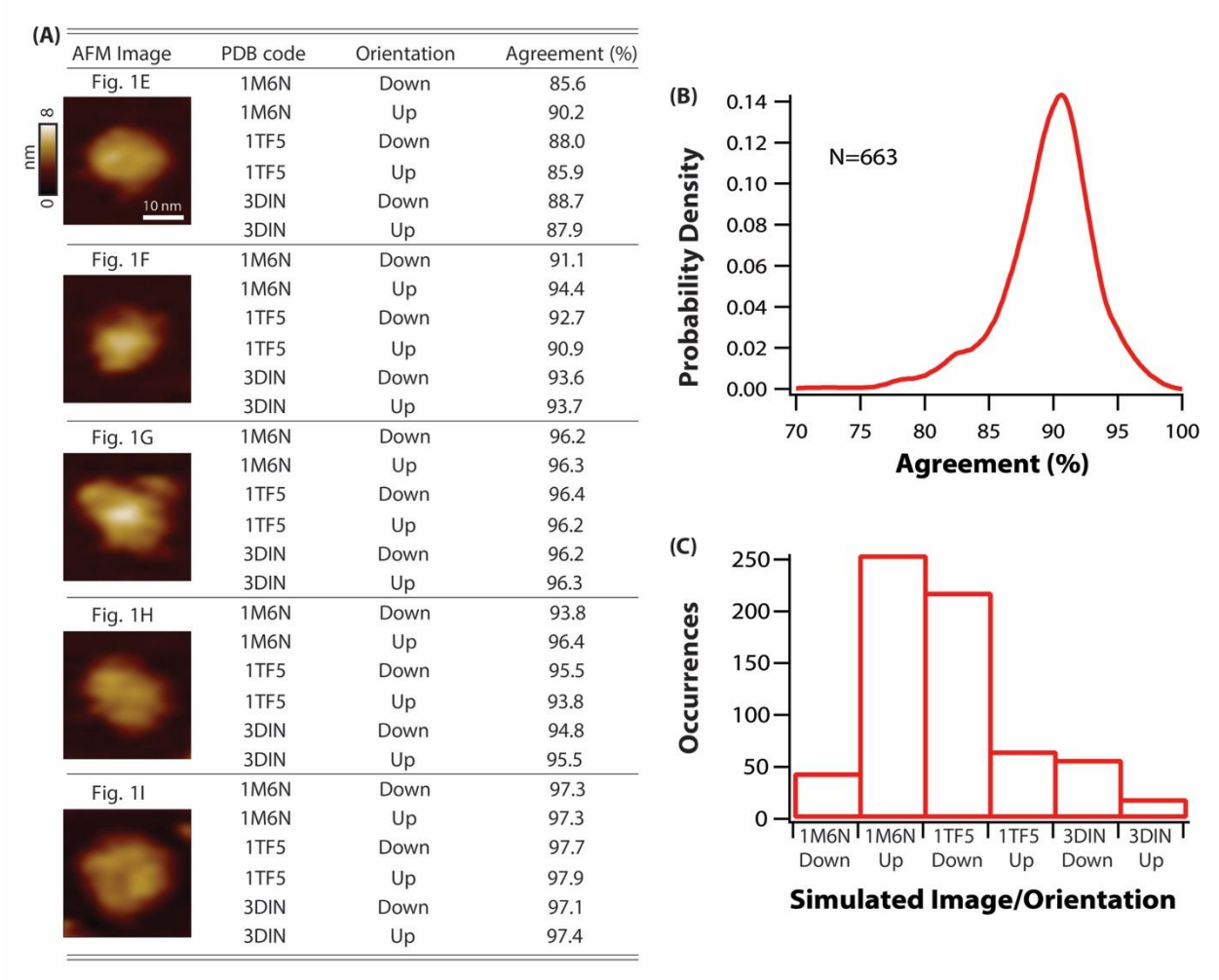

Fig. S3. AFM image data corroborate with simulations. (**A**) Comparison of five AFM images (Fig. 1E-I) to simulated images (fig. S2) based on crystal structures (protein data bank (PDB) codes listed) in the up and down orientations (defined in fig. S2). (**B**) Smoothed histogram showing the results of agreement analysis between a subset of $N = 663$ SecA-WT molecules in the apo condition and the same six simulated images. The data indicate that most of the AFM images are in good agreement (around 90%) with at least one of the simulated images. Here we plot only the maximum agreement between any of the six simulated images for each experimental image. (**C**) Shows the number of occurrences that a specific crystal/orientation achieved maximum agreement out of all six possible crystals/orientations. AFM data were most similar to simulated images of "wide open" conformation (1M6N) in the up orientation and "open" conformation (1TF5) in the down orientation.

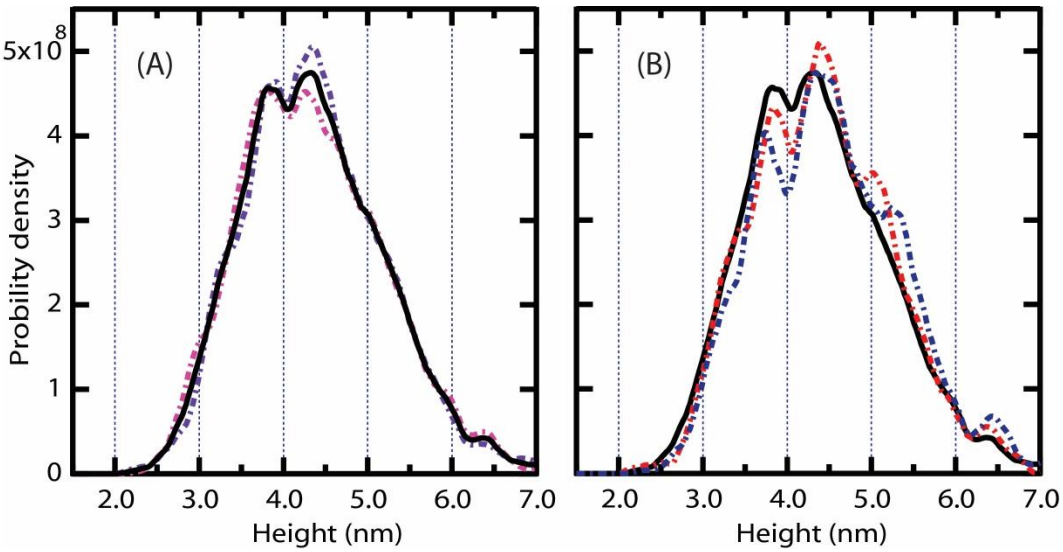

Fig. S4. Statistically robust subpopulations. (A) Height histogram of SecA-WT (black, N = *3726*) and two randomly culled subsets to $N/2$ (*dashed traces*) are shown. **(B)** Height histograms from two independent experiments (*dashed*) are compared to the summary histogram (*black*). This analysis verifies the presence of stable sub-populations.

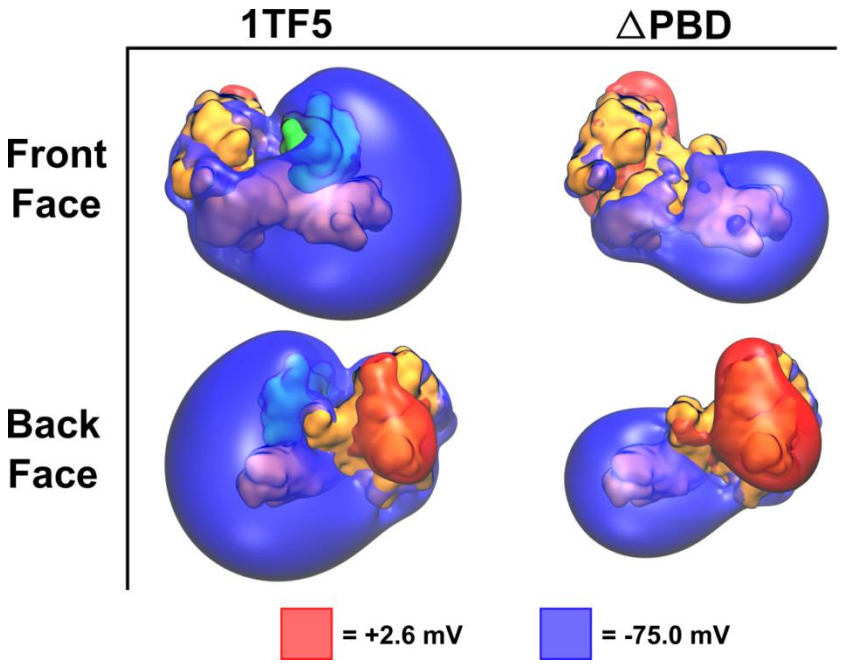

Fig. S5. Equipotential surfaces comparing the front and back faces of SecA. Surfaces of constant electrostatic potential at pH=7, generated from crystal structure 1TF5 and 1TF5 with the protein binding domain deleted (ΔPBD). Shown are views of the front and back faces of SecA (defined in fig. S2), which are likely to be oriented upwards towards the AFM tip during imaging. For both SecA species, the negative cloud on the front face is much larger in magnitude than the positive cloud on the back face; additionally both of the back faces have a slight di-polar nature. The data indicate that deleting the protein binding domain leads to an overall reduction of the negative potential, but asymmetry between the faces is preserved. This analysis suggests that the ΔPBD mutation is not likely to alter the overall orientation of SecA when adsorbed onto mica. This is consistent with our AFM observations.

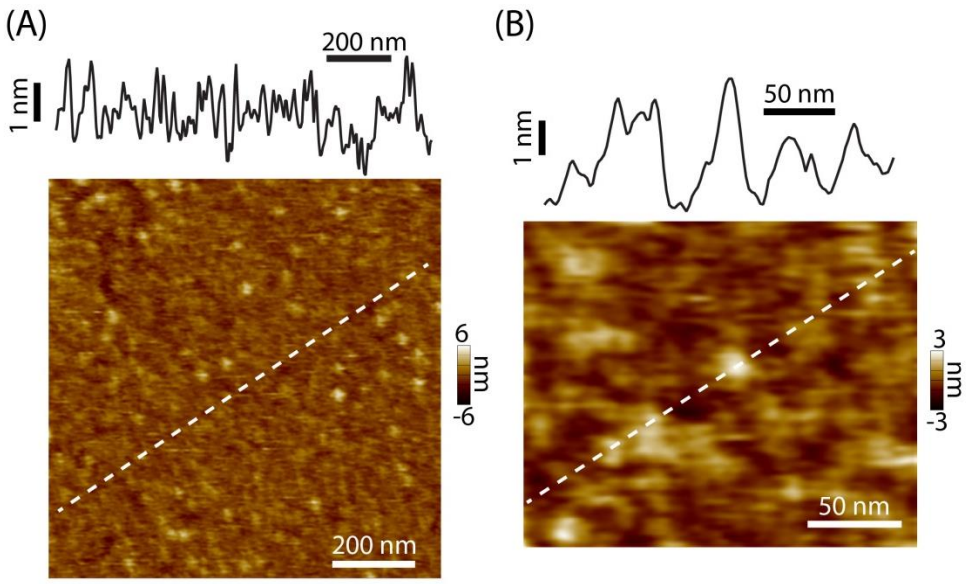

Fig. S6. Evaluation of molecular density of SecA prepared for surface-adsorbed ATPase activity assays. (**A**) AFM image of SecA prepared for surface-based ATPase measurements. Note, the incubation concentration used in this assay was 100-fold higher than that used for AFM analysis. Panel (**B**) shows a detailed view. Images were acquired in the presence of 3 mM ATP, line scans (*dashed*) are shown above each image. Under these conditions, the packing density of SecA prevents the tip from reaching the underlying mica in most areas. This observation suggests that the SecA has formed a continuous tightly-packed monolayer over the mica disk (radius ~5 mm). Based on the crystallographic dimensions of SecA and the likely orientation of the molecule on the surface (fig. S2) we estimate a per-molecule area footprint of approximately 4800 $Å^2$ and hence, calculate there to be about 3×10^{-12} mol SecA on the mica. We note that this per-molecule area is smaller than the AFM image area because it does not account for tip convolution.

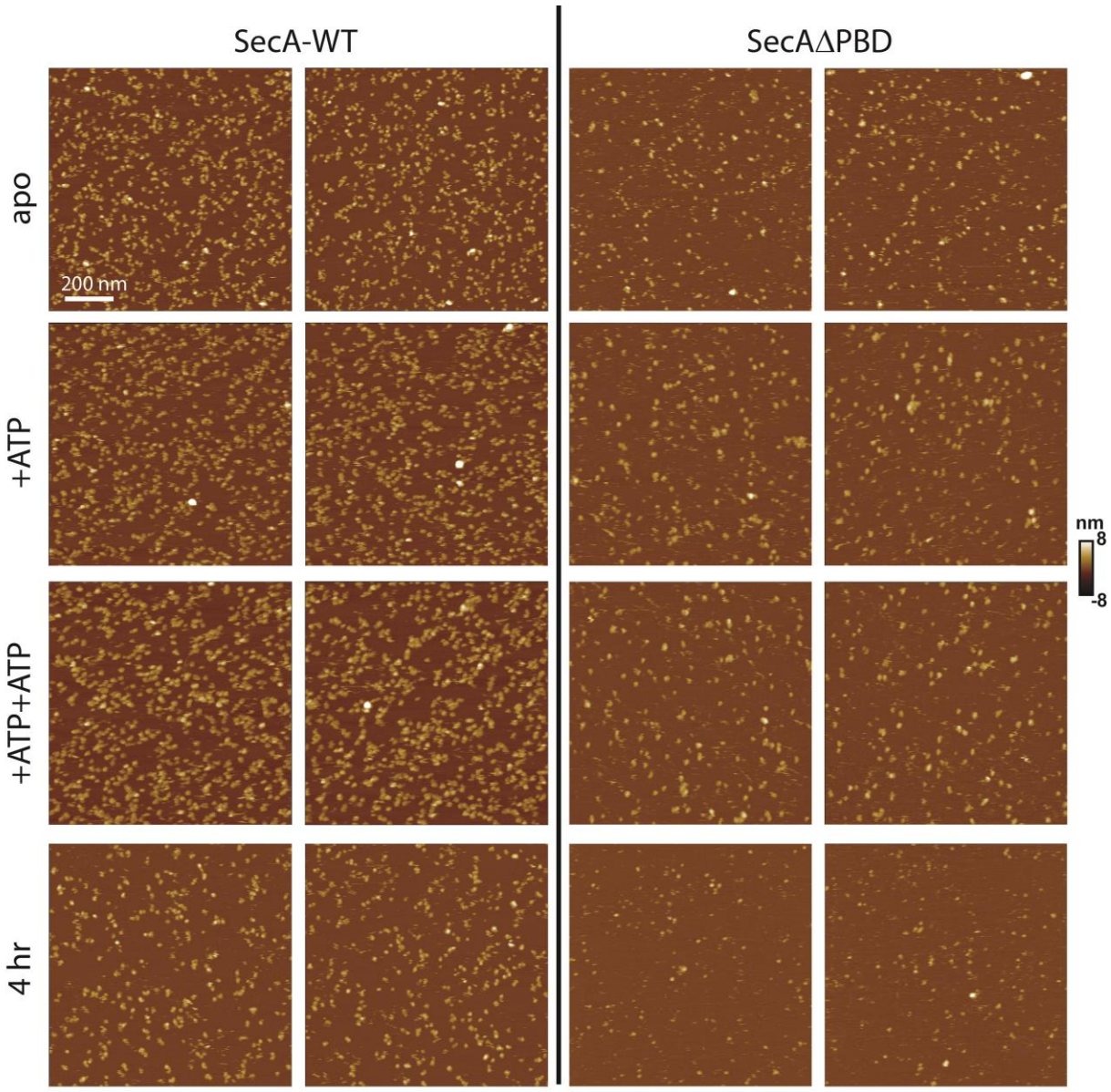

Fig. S7. Representative images of SecA-WT and SecAΔPBD subject to different conditions. apo = not exposed to any nucleotide after purification; +ATP = pre-incubated with 100 μM ATP for 15 min prior to deposition on mica and then imaged in the absence of ATP; +ATP+ATP = pre-incubated with 100 μM ATP in solution for 15 min and then imaged with 100 μM ATP in the imaging buffer; and 4 hr = pre-incubated with 100 μM ATP in solution for 4 hours and then imaged in the absence of ATP in the imaging buffer.

Table S1. Statistics of SecA-WT (WT) and SecAΔPBD (ΔPBD) area distributions in the following conditions. (*i*) apo = not exposed to any nucleotide after purification; (*ii*) +ATP = pre-incubated with 100 μM ATP for 15 min prior to deposition on mica and then imaged in the absence of ATP; (*iii*) +ATP+ATP = pre-incubated with 100 μM ATP in solution for 15 min and then imaged with 100 μM ATP in the imaging buffer; and (*iv*) 4 hr = pre-incubated with 100 μM ATP in solution for 4 hours and then imaged in the absence of ATP in the imaging buffer. We show the number of features included in the analysis *N*; the mean area footprint ± standard error of the mean; as well as the peak area ± error, as determined via the most populated bin in the area histogram ± the bin width.

Assay	*N* - WT	Mean Area WT [nm^2]	Peak Area WT [nm^2]	*N* - ΔPBD	Mean Area ΔPBD [nm^2]	Peak Area ΔPBD [nm^2]
(i) apo	3726	480 ± 6	200 ± 10	4009	380 ± 4	230 ± 10
(ii) +ATP	3376	650 ± 9	270 ± 10	1907	580 ± 9	230 ± 10
(iii) +ATP+ATP	2437	940 ± 17	300 ± 10	1458	570 ± 9	300 ± 10
(iv) 4 hr	2448	450 ± 6	280 ± 10	1061	330 ± 8	235 ± 10

Table S2. Mean height (±SEM) and FWHM of the SecA-WT and the SecAΔPBD mutant height distributions in different conditions.

ATP Assay	*N* - WT	Mean Height WT [Å]	FWHM WT [Å]	*N* - ΔPBD	Mean Height ΔPBD [Å]	FWHM ΔPBD [Å]
(i) apo	3726	44 ± 0.2	20	4009	42 ± 0.2	17
(ii) +ATP	3376	41 ± 0.2	21	1907	36 ± 0.2	15
(iii) +ATP+ATP	2437	44 ± 0.3	23	1458	39 ± 0.3	15
(iv) 4 hr	2448	38 ± 0.2	16	1061	34 ± 0.3	14

Table S3. Statistics of the SecA-WT and SecAΔPBD area distributions after exposure to ADP or ADP-AlF$_3$. We show the number of features included in the analysis *N*; the mean area footprint ± standard error of the mean; as well as the peak area ± error, as determined via the most populated bin in the area histogram ± the bin width.

Nucleotide	*N*-WT	Mean Area WT [nm^2]	Peak Area WT [nm^2]	*N*-ΔPBD	Mean Area ΔPBD [nm^2]	Peak Area ΔPBD [nm^2]
ADP	6428	420 ± 4	220 ± 10	3104	390 ± 5	220 ± 10
ADP-AlF$_3$	4590	360 ± 4	235 ± 10	2159	320 ± 6	220 ± 10

Table S4. Mean height (±SEM) and FWHM of the SecA-WT and the SecAΔPBD mutant distributions exposed to ADP and ADP-AlF$_3$.

Nucleotide	*N* - WT	Mean Height WT [Å]	FWHM WT [Å]	*N* - ΔPBD	Mean Height ΔPBD [Å]	FWHM ΔPBD [Å]
ADP	6428	42 ± 0.2	18	3104	42 ± 0.2	17
ADP-AlF$_3$	4590	40 ± 0.2	15	2159	37 ± 0.3	16

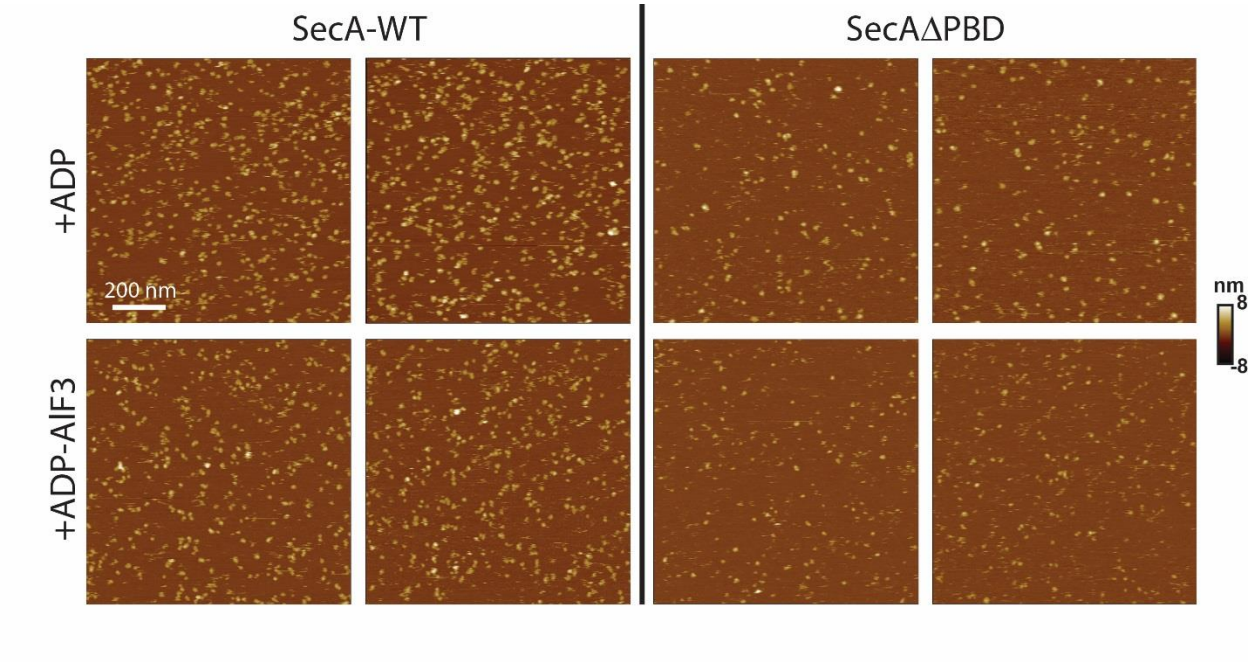

Fig. S8. Representative images of SecA-WT and SecAΔPBD exposed to different nucleotides. Enzymes were exposed to ADP or ADP-AlF_3 for 15 mins prior to imaging, and then imaged in the absence of nucleotides.

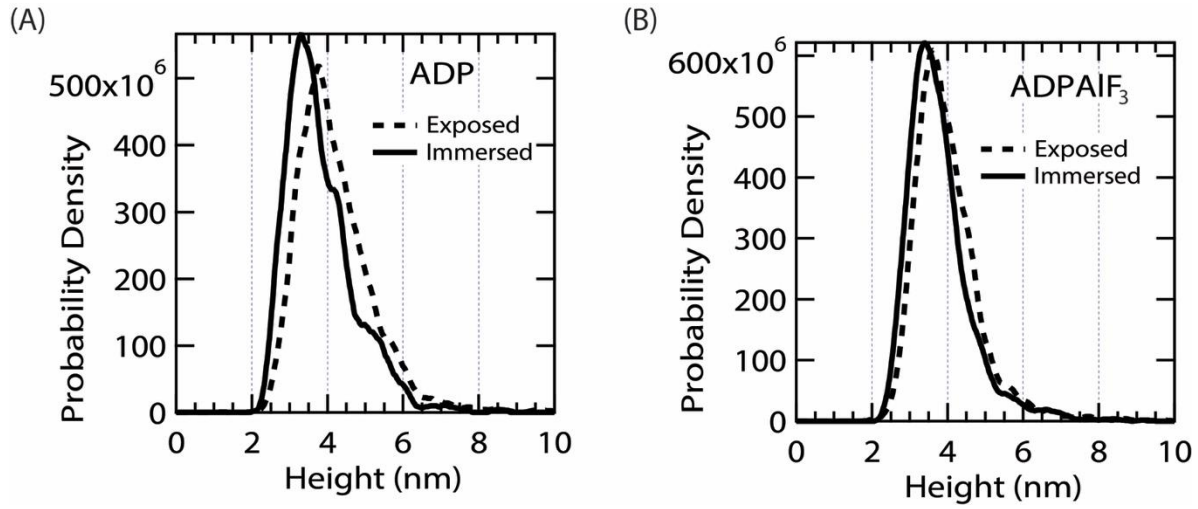

Fig. S9. Height histograms of SecA immersed in and exposed to nonhydrolyzable nucleotides. (**A**) Comparison of height histograms for SecA-WT when imaged in (*solid line*, N = 1090) or just after exposure to (*dashed*, N = 6428) ADP. (**B**) Analogous data for ADP-AlF_3 (Immersed: N = 1561; Exposed: N = 4590). These data indicate that the presence of the nucleotides in the AFM imaging buffer results in slight downward height shifts of 4 or 2 Å, for ADP and ADP-AlF_3, respectively.

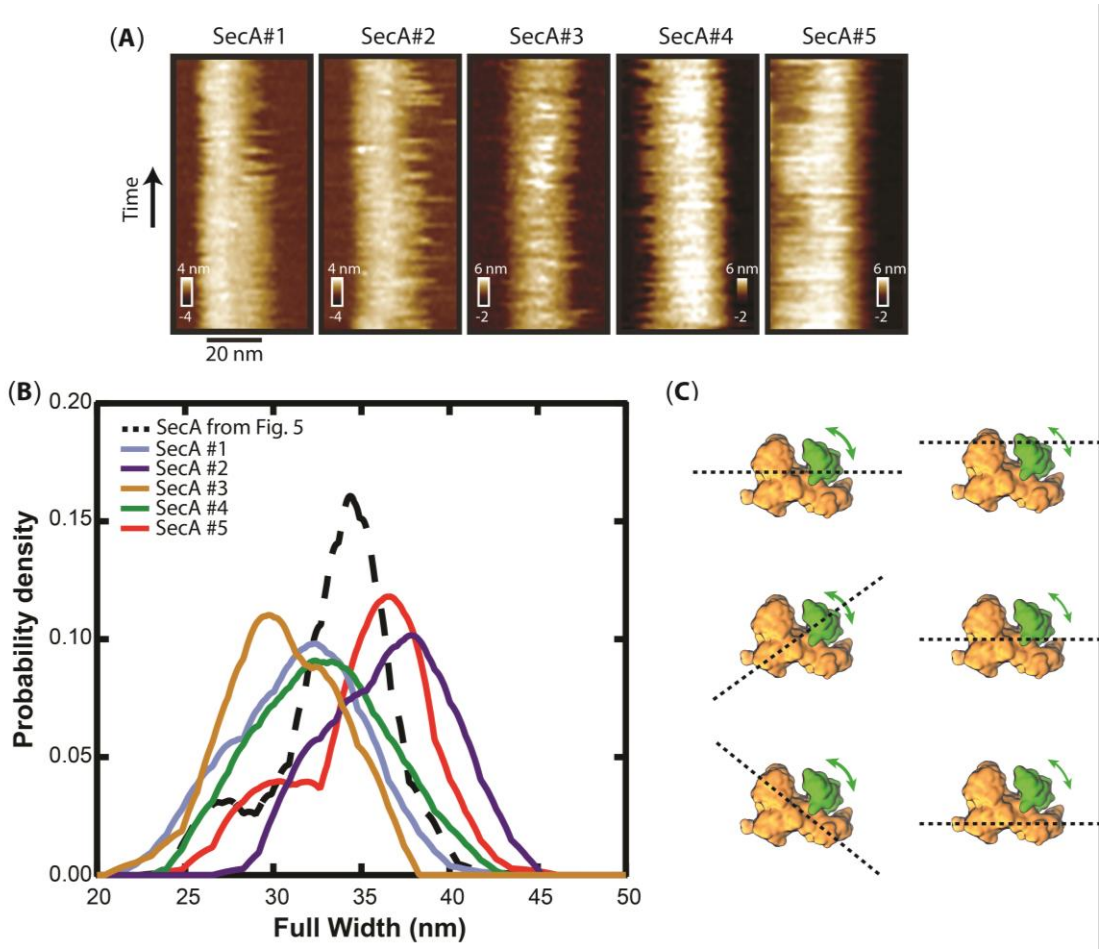

Fig. S10. Additional kymograph data. (**A**) Kymograph segments (temporal duration 12.4 s) of five distinct SecA-WT molecules in the presence of saturating ATP. (**B**) Histograms showing the full width distribution of each molecule. The number of line scans evaluated: $N = 125$, 64, 64, 75, and 75, for SecA#1–5, respectively. Data from Fig. 5 is carried over for reference (dashed). (**C**) Cartoons (drawn with the front face "up" orientation, defined in fig. S2) demonstrate variations due to angular (left column) and translational (right column) offsets on the resulting one-dimensional scanning measurements (*dashed lines*). Certain scan trajectories are better suited to observe protein binding domain (*green*) dynamics. Despite variations, evidence of at least two states ('compact' and 'extended') can be observed in the data.